Adiabatic state preparation of stripe phases with strongly magnetic atoms

Azadeh Mazloom,[1,2,3] Benoît Vermersch,[2,3] Mikhail A. Baranov,[2,3] and Marcello Dalmonte[2,4]
[1]*Department of Physics, Institute for Advanced Studies in Basic Sciences, Zanjan 45137-66731, Iran*
[2]*Institute for Theoretical Physics, University of Innsbruck, A-6020 Innsbruck, Austria*
[3]*Institute for Quantum Optics and Quantum Information, Austrian Academy of Sciences, A-6020 Innsbruck, Austria*
[4]*Abdus Salam International Centre for Theoretical Physics, Strada Costiera 11, I-34151 Trieste, Italy*
(Received 30 May 2017; published 1 September 2017)

We propose a protocol for realizing the stripe phase in two spin models on a two-dimensional square lattice, which can be implemented with strongly magnetic atoms (Cr, Dy, Er, etc.) in optical lattices by encoding spin states into Zeeman sublevels of the ground-state manifold. The protocol is tested with cluster-mean-field time-dependent variational *Ansätze*, validated by comparison with exact results for small systems, which enable us to simulate the dynamics of systems with up to 64 sites during the state-preparation protocol. This allows us, in particular, to estimate the time required for preparation of the stripe phase with high fidelity under real experimental conditions.

DOI: 10.1103/PhysRevA.96.033602

I. INTRODUCTION

Experiments with ultracold quantum gases of atoms and molecules have recently witnessed tremendous progress in realizing and probing many-body physics with long-range interacting spin systems [1]. Several works have reported the observation of coherent dynamics with both magnetic and Rydberg atoms [2,3] and polar molecules [1], ranging from the time evolution of spin models after a quantum quench [4–7] to the realization of Hubbard and extended Bose-Hubbard models featuring both local and nonlocal interactions [8–11]. These experimental studies are paving the way for the investigation of quantum magnetism in atomic and molecular quantum systems, in particular, the stability of ordered magnetic phases in frustrated systems [1,2].

One example of such phases is the stripe phase supporting ferromagnetic order along one direction and antiferromagnetic order along the perpendicular one. Stripe order has been widely discussed in quantum magnetism in the context of both spin (Heisenberg and Ising types) [12,13] and fermionic (Hubbard and t-J) models (with possible implications for the finite-doping phases of high-temperature superconductors) [14]. Moreover, stripe ordering represents a natural counterpart to antiferromagnets in the presence of angle-dependent interactions [12]: these interactions do naturally occur in dipolar gases of magnetic atoms such as Cr, Dy, and Er, all of which are by now being observed in quantum degenerate regimes [15–19]. The main virtues of such atomic species are that they can combine dipolar interactions with close-to-ideal initial-state preparation (such as Mott insulators with unit filling) and long coherence times (of the order of 1 s) which compare well with the interaction time scales (typically of the order of 10 to 100 Hz in units of $\hbar$) [1,2]. These two features make magnetic atoms an ideal platform for the realization and investigation of stripe phases in atomic many-body systems, an approach very complementary to recent experimental findings [20] in the context of spin-orbit-coupled Bose gases [21,22].

One of the key questions toward the realization of such magnetic phases is the identification of clear-cut state-preparation protocols which can warrant experimental observability of specific signatures (i.e., correlation functions) under realistic experimental conditions. In this work, we address the preparation of the stripe phase in spin-1 Heisenberg-type and spin-1/2 Ising-type models on the square lattice, with antiferromagnetic interactions between neighbors in one direction and ferromagnetic interactions along the other, which can be realized with magnetic atoms trapped in optical lattices. For both models, the proposed adiabatic protocols for preparing the stripe phase are tested using a time-dependent variational principle directly inspired by (cluster) mean-field theory. This method agrees well with the exact treatment of small systems and allows us to tackle the full time-dependent dynamics for lattices containing of the order of 100 sites, which is comparable to the largest, defect-free Mott-insulator states available in current experiments [23]. Our results strongly indicate that the realization of the stripe phases is within reach of current experiments with strongly magnetic atoms such as Dy and Er, with strong signatures of the stripe formation already visible for moderate speeds of changes in the system's parameters during the preparation protocols. Beyond the magnetic atom implementation discussed here, our findings are also applicable to other physical systems, such as polar molecules and Rydberg atoms in optical lattices [2] and arrays of superconducting circuits [24,25], which are described by very similar lattice spin Hamiltonians.

The structure of this paper is as follows. In Sec. II, we discuss the two dipolar spin models of interest. In Sec. III, we introduce the time-dependent variational principle and discuss in detail the state-preparation protocols for stripe phases in both spin-1/2 and spin-1 models. Section IV contains two implementation schemes using magnetic atoms in optical lattices and provides a glimpse of the corresponding experimental time scales for both coherent and incoherent (dissipation) dynamics. Finally, we draw our conclusions in Sec. V.

II. MODEL HAMILTONIANS

In this section we introduce two spin models of interacting dipoles whose phase diagrams include stripe phases. The setup we have in mind is shown in Fig. 1(a). It contains magnetic atoms at fixed positions on a square lattice, interacting via dipole-dipole interactions (DDIs) and with an external magnetic field along the z axis. This is the common starting point

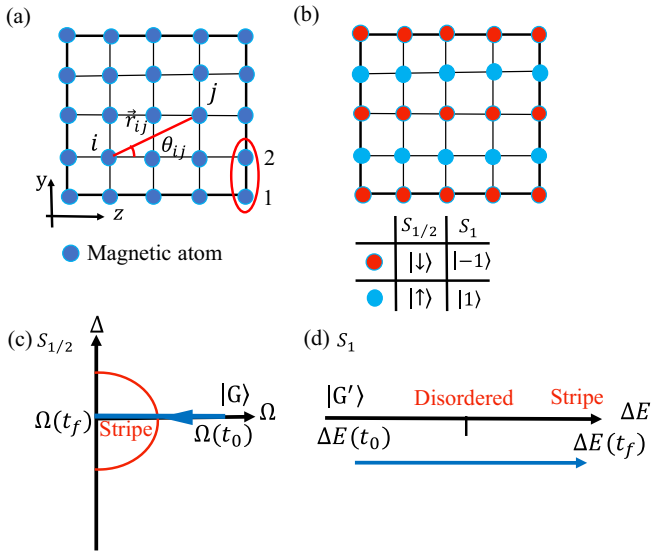

FIG. 1. (a) The arrangement of dipoles on a square lattice with a single atom per site; $\vec{r}_{ij}$ is the relative vector between spins i and j, and θ_{ij} is the angle between $\vec{r}_{ij}$ and the quantization axis z. (b) Representation of the stripe phase formed by aligned dipoles in direction z and antialigned ones in direction y. (c) The schematic phase diagram of the ground state of the spin-1/2 model in Δ-Ω space. The blue arrow shows the sweep path along which the ground state of the system adiabatically changes from a ferromagnetic phase $|G\rangle$ at $\Omega(t_0) \gg |C_{ij}|$ and $\Delta(t_0) = 0$ to the stripe phase at $\Omega(t_f) = 0$ and $\Delta(t_f) = 0$. (d) Different phases of the spin-1 model as a function of ΔE. The stripe phase can be prepared by a slow change in ΔE along the sweep path shown as the blue arrow.

for the realization of both spin-1/2 and spin-1 lattice models. In the following we discuss the corresponding Hamiltonians and the phase diagrams. For the implementation of the models, we refer the reader to Sec. IV.

A. Spin-1/2 model

The first model we consider is obtained by assuming the two involved atomic states as states $|\uparrow\rangle, |\downarrow\rangle$ of pseudo-spin-1/2 particles. The corresponding Hamiltonian reads

$$H = \sum_{i<j}^{N} C_{ij}\sigma_z^{(i)}\sigma_z^{(j)} + \Omega\sum_{i}^{N}\sigma_x^{(i)} - \Delta\sum_{i}^{N}\sigma_z^{(i)}, \qquad (1)$$

where N is the number of atoms and $\sigma_z^{(i)} = |\uparrow\rangle_i\langle\uparrow|_i - |\downarrow\rangle_i\langle\downarrow|_i$ and $\sigma_x^{(i)} = |\uparrow\rangle_i\langle\downarrow|_i + |\downarrow\rangle_i\langle\uparrow|_i$ are the Pauli matrices acting at site i. The first term in this Hamiltonian describes the Ising-type DDI between two spins on sites i and j with $C_{ij} = c_d(1 - 3\cos^2\theta_{ij})/r_{ij}^3$, where the interaction constant c_d depends on the specific implementation of the spin models, $r_{ij} = |\mathbf{r}_i - \mathbf{r}_j|$ is the distance (in units of the lattice spacing a) between the sites, and θ_{ij} is the corresponding angle with respect to the quantization axis z [see Fig. 1(a)]. In order to have the stripe phase as the ground state, we place the quantization axis in the plane of the atoms such that the DDI is attractive in one direction ($\theta_{ij} = 0$) and repulsive in the other direction ($\theta_{ij} = \pi/2$) [26]. Finally, the last two terms in Eq. (1) correspond to transverse (Ω) and longitudinal (Δ) magnetic fields, which will be used for the state preparation.

The zero-temperature phase diagram of the Hamiltonian (1) is schematically shown in Fig. 1(c). It hosts a stripe phase for $|\Omega|, |\Delta| < |c_d|$ with spins aligned along the z axis and antialigned along the y axis, as shown in Fig. 1(b). This phase is destroyed by increasing magnetic fields when $|\Omega|, |\Delta| \sim |c_d|$ (see [27–29] in the context of Rydberg atoms), and for $|\Omega|, |\Delta| \gg |c_d|$ the system is in the ferromagnetic phase with spins oriented along the total magnetic field [30]. In particular, for $\Omega \gg \Delta, |C_{ij}|$, all spins align preferentially along the x axis, resulting in the ground state $|G\rangle = |\rightarrow\rangle_1 \cdots |\rightarrow\rangle_N$, with $|\rightarrow\rangle = (|\uparrow\rangle - |\downarrow\rangle)/\sqrt{(2)}$.

B. Spin-1 model

The second model is for spin-1 particles, with three internal atomic states representing the spin-1 states $|-1\rangle$, $|0\rangle$, and $|1\rangle$ (see Sec. IV for details), described by the following Hamiltonian:

$$\begin{aligned} H = {} & \Delta E\sum_{i}^{N}\left(1 - S_z^{(i)^2}\right) + \sum_{i<j}^{N} C_{ij}S_z^{(i)}S_z^{(j)} \\ & + \sum_{i<j}^{N} C_{ij}\left[\gamma S_+^{(i)}\left(S_z^{(j)} + S_z^{(i)}\right)S_-^{(j)} + \beta S_+^{(i)}S_-^{(j)}\right. \\ & \left. + \delta S_+^{(i)}S_z^{(i)}S_z^{(j)}S_-^{(j)} + \text{H.c.}\right], \end{aligned} \qquad (2)$$

where N is the number of spins; $S_z^{(i)} = |1\rangle_i\langle 1|_i - |-1\rangle_i\langle -1|_i$, $S_+^{(i)} = \sqrt{2}(|1\rangle\langle 0| + |0\rangle\langle -1|)$, and $S_-^{(i)} = (S_+^{(i)})^\dagger$ are spin-1 operators; and β, γ, and δ are constants depending on chosen atomic states in the implementation scheme (see Sec. IV C). The first term in this Hamiltonian is the energy difference between state $|0\rangle$ and states $|\pm 1\rangle$, which serves as a controlling parameter during state preparation. The last two terms represent the DDI including a XXZ-type Hamiltonian (the second term) and higher-order spin operators (the last term). Obviously, state $|G'\rangle = |0\rangle_1 \cdots |0\rangle_N$ minimizes the energy of the Hamiltonian for large negative ΔE, $\Delta E \ll -|C_{ij}|$. For small ΔE ($|\Delta E| \ll |C_{ij}|$), the spin exchange term of the Hamiltonian leads to a disordered phase (Fig. 1). Finally, for large positive ΔE, $\Delta E \gg |C_{ij}|$, the DDI arranges spins into the stripe phase.

III. DYNAMICAL PREPARATION OF THE STRIPE PHASE

We now proceed with the description of the stripe-phase preparation protocols for both of the above models, which is based on the adiabatic evolution of the ground state [7,29,31,32]. This is achieved by changing adiabatically the magnetic field from the values at which the ground state is simple and easily realizable in experiments to the values at which the stripe phase is the ground state. To characterize the state of the system during the protocol, we introduce the stripe order parameters along the z and y lattice directions [see Fig. 1(b)],

$$M_z = \frac{1}{N}\sum_i \left\langle S_z^{(i)}S_z^{(i+1_z)}\right\rangle, \quad M_y = \frac{1}{N}\sum_i \left\langle S_z^{(i)}S_z^{(i+1_y)}\right\rangle, \qquad (3)$$

where $S_z^{(i)}$ are the spin operators of the corresponding model ($S_z^{(i)} \to \sigma_z^{(i)}$ for the spin-1/2 case) and 1_α represents a shift by one site along the α direction. The system is in the stripe phase when $M_z \to 1$ and $M_y \to -1$.

A. Dynamical state preparation of stripe phases for the spin-1/2 model

For the spin-1/2 model, we consider initially (at time $t = t_0$) the system with $\Delta(t_0) = 0, \Omega(t_0) \gg |c_d|$ in its ground state $|G\rangle$, which can be experimentally prepared with high fidelity, and then adiabatically decrease Ω to reach the final point $\Delta(t_f) = 0, \Omega(t_f) = 0$ at time t_f, where the stripe phase is the ground state. Note, however, that during the parameter ramp, we cross the phase-transition point. Therefore, strictly speaking, the criterion of adiabaticity can be fulfilled only in a finite system where the finite-size effects ensure the existence of a finite gap even at the transition point. Nevertheless, keeping in mind that experimental realizations with cold atoms always deal with finite systems, this does not cause any real problems but requires the entire time $t_f - t_0$ of the preparation protocol be sufficiently large in order to minimize the population of excited states along the ramp (see below).

We test the protocol with an approach based on a time-dependent variational principle (TDVP) which allows us to simulate the dynamics of the system with a large number of atoms [29,33]. This makes it possible, in particular, for us to estimate the minimal coherence time needed to obtain the stripe phase experimentally with good fidelity. The justification for our approach is based on the comparison with the results of exact diagonalization for small systems.

Within the TDVP approach, the time evolution of a many-body quantum state of the spin-1/2 model is described via a product-state wave function,

$$|\Phi\rangle = \prod_{i=1}^{N} [\alpha_i(t)|\uparrow\rangle_i + \beta_i(t)|\downarrow\rangle_i], \tag{4}$$

where $\alpha_i(t)$ and $\beta_i(t)$ are the time-dependent coefficients satisfying the normalization condition $|\alpha_i|^2 + |\beta_i|^2 = 1$. Note that the ground state of the Hamiltonian (1) with $\Delta = 0$ in the classical limit $\Omega \to 0$ (the stripe phase) is described by this *Ansatz* with the red and blue circles in Fig. 1(b), which correspond to $|\alpha_i|^2 = 1, \beta_i = 0$ and $\alpha_i = 0, |\beta_i|^2 = 1$, respectively. Our mean-field (MF) *Ansatz*, however, neglects the quantum pair correlation in the nonclassical limit, $\Omega \neq 0$.

The time evolution of variational coefficients $\alpha_i(t)$ and $\beta_i(t)$ with changing Ω and Δ can be calculated by the Euler-Lagrange equations [29]

$$\frac{d}{dt}\left(\frac{\partial L}{\partial \dot{\alpha}_i^*}\right) = \frac{\partial L}{\partial \alpha_i^*}, \tag{5}$$

$$\frac{d}{dt}\left(\frac{\partial L}{\partial \dot{\beta}_i^*}\right) = \frac{\partial L}{\partial \beta_i^*}, \tag{6}$$

where L is the Lagrangian of the system,

$$L = \frac{i}{2}(\langle\Phi|\dot{\Phi}\rangle - \langle\dot{\Phi}|\Phi\rangle) - \langle\Phi|H|\Phi\rangle. \tag{7}$$

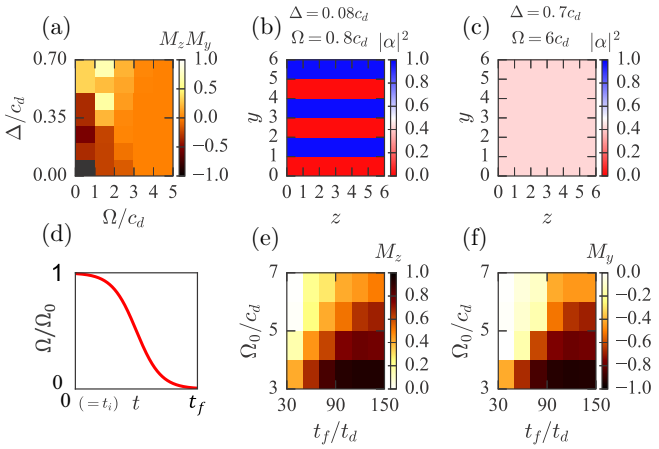

FIG. 2. The ground state of the spin-1/2 model on a 6×6 lattice and the preparation of the stripe phase. (a) The order parameter of the system M_zM_y as a function of Δ and Ω, indicating the stripe phase for small Δ and Ω. The occupation of state $|\uparrow\rangle$ is shown in (b) for small Δ and Ω, representing the stripe phase, and (c) for large Δ and Ω, indicating a ferromagnetic phase. (d) The variation of Ω with time ($t_d = \hbar/c_d$) during the preparation protocol and the resulting spin-spin correlations (e) M_z and (f) M_y at the end of the protocol as a function of the preparation time t_f and the initial value of Ω_0.

After substituting the MF *Ansatz* (4) and the Hamiltonian (1) into Eq. (7), the Euler-Lagrange equations (5) and (6) give

$$-i\dot{\alpha}_i = \left[-\Delta(t) + \sum_j C_{ij}(|\beta_j|^2 - |\alpha_j|^2)\right]\alpha_i - \Omega(t)\beta_i, \tag{8}$$

$$-i\dot{\beta}_i = \left[\Delta(t) + \sum_j C_{ij}(|\alpha_j|^2 - |\beta_j|^2)\right]\beta_i - \Omega(t)\alpha_i. \tag{9}$$

For $C_{ij} = 0$, Eqs. (8) and (9) describe the single-spin Rabi oscillations with the frequency $\sqrt{\Delta^2 + \Omega^2}$. We see that the interactions C_{ij} in the MF description generate nonlinear corrections to the longitudinal magnetic field Δ, so that the rate of local spin flips depends on the spin configuration on the neighboring sites.

The *Ansatz* in Eq. (4) can also be used to investigate the ground state of the system by considering the parameters α_i and β_i as independent variational parameters (subject to only the normalization constraint) and minimizing the energy of the system. In Fig. 2(a) we present the results of such calculations for a 6×6 lattice by showing the quantity M_zM_y as a function of Δ and Ω. As expected, the stripe phase ($M_zM_y \to -1$) is the variational ground state of the system when the DDI is larger than the transverse and longitudinal magnetic fields Δ and Ω [see Fig. 2(b)]. With increasing magnetic fields, the stripe phase disappears [Fig. 2(c)], and for large Ω and Δ the ground state is the ferromagnetic one [for the parameters in Fig. 2(c), the spins are mostly oriented in the x direction, $S_x = N^{-1}\sum_i \langle\sigma_x^{(i)}\rangle = -0.96$].

We now analyze the dynamical preparation of the stripe phase along the trajectory shown in Fig. 1(b) with $\Delta = 0$ for

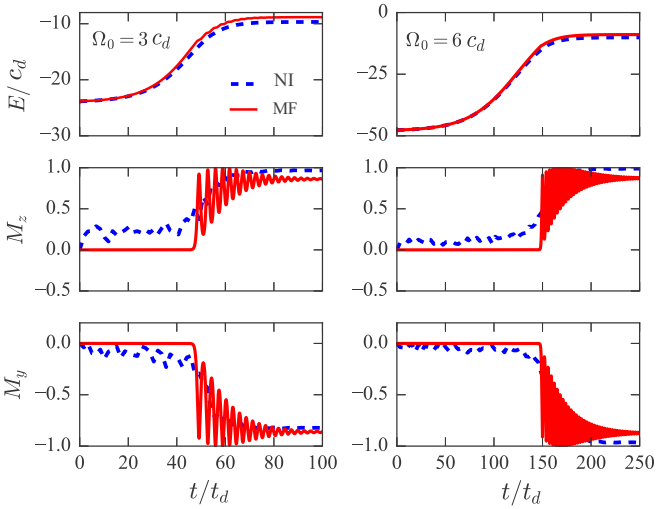

FIG. 3. Comparison of the results of the dynamical MF approach (solid lines) with the exact solution of the time-dependent Schrödinger equation (dashed lines) for a 4×4 lattice. Time evolution ($t_d = \hbar/c_d$) of the energy (top), M_z (middle), and M_y (bottom) for different values of Ω_0.

all times and Ω decreasing from its initial value $\Omega = \Omega_0$ to zero, as represented in Fig. 2(d). For the system initialized in state $|G\rangle = |{\rightarrow}\rangle_1 \cdots |{\rightarrow}\rangle_N$, with $|{\rightarrow}\rangle = (|{\uparrow}\rangle - |{\downarrow}\rangle)/\sqrt{2}$, Figs. 2(e) and 2(f) present the final values of M_z and M_y as a function of Ω_0 and t_f. We see that the larger initial value Ω_0 is, the longer it takes to reach the stripe phase with high fidelity. For $\Omega_0 = 3c_d$ the stripe phase is reached already for $t_f \sim 10^2 t_d$, where $t_d = \hbar/c_d$.

To validate our MF approach we compare it with the exact numerical solutions of the time-dependent Schrödinger equation for the same initial state $|G\rangle = |{\rightarrow}\rangle_1 \cdots |{\rightarrow}\rangle_N$ on the 4×4 lattice ($N = 16$). The comparison is presented in Fig. 3 and shows that the two methods are in very good agreement when comparing the energy. The order parameters (spin-spin correlators) $M_{z,y}$ are in agreement within 10% for all times except those close to the transition point, where the TDVP simulations show strong oscillations. They correspond to a large-amplitude motion of the system over a practically flat potential landscape in the low-energy manifold of states near the transition. Away from the transition point, when the system chooses one of the two possible stripe configurations (see also the discussion below), the oscillations disappear. In contrast, the numerical solutions of the Schrödinger equation do not show any noticeable oscillations. We attribute this difference to the fact that the evolution within the *Ansatz* (4) allows us to reach only a very limited (compared to the true quantum-mechanical evolution) part of the Hilbert space, making impossible the smearing out of the total contribution of various oscillating terms in the spin-spin correlation functions.

In Fig. 4, we plot the evolution of the occupation probabilities of states $|{\uparrow}\rangle$ (red curve) and $|{\downarrow}\rangle$ (black curve) to illustrate the dynamics of the formation of the stripe pattern within the TDVP. It is important to mention that within the TDVP the system chooses spontaneously one of the two possible stripe configurations. We believe that this spontaneous symmetry breaking is a result of finite numerical precision

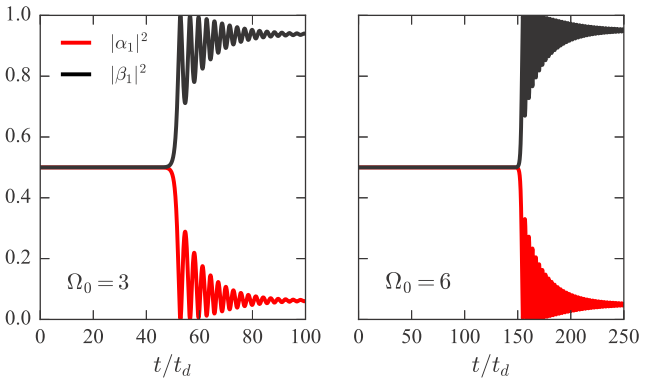

FIG. 4. Time evolution of the occupation of states $|{\uparrow}\rangle$ (red line) and $|{\downarrow}\rangle$ (black line) in a lattice site and for different values of Ω_0.

during the calculation. In contrast, our numerical integration of the time-dependent Schrödinger equation always results in a superposition of the two possible stripe configurations, showing therefore no sign of spontaneous symmetry breaking. Such "robustness" of the numerical solutions of the Schrödinger equation is due to the quantum correlations (entanglement) over a large part of the Hilbert space, which is built in the system during the purely quantum-mechanical time evolution. In real physical systems, however, decoherence processes (due to finite temperature, noise, etc.) destroy most of these correlations and cause spontaneous symmetry breaking.

As a final comment we note that, as we have already seen in Fig. 2, the larger Ω_0 is, the longer ramps are required to prepare the stripe phase.

B. Dynamical state preparation of stripe phases for the spin-1 model

For the preparation of the stripe phase within the spin-1 model (2), we start with $\Delta E_0 = \Delta E(t_i) \ll -|C_{ij}|$ in the Hamiltonian and initialize the system in state $|G'\rangle = |0\rangle_1 \cdots |0\rangle_N$. We then increase ΔE adiabatically to a large positive value $\Delta E_f = \Delta E(t_f) \gg |C_{i,j}|$ [see Fig. 1(d)] to end up in the stripe phase formed on the manifold of spin states $|1\rangle_i$ and $|-1\rangle_i$ (the spin states $|0\rangle_i$ are effectively eliminated by the large positive ΔE_f).

Before proceeding to the analysis of the time evolution of the system under the ramp we note that the MF variational *Ansatz* used above for the spin-1/2 model cannot be applied here because it is unable to describe the flip-flop processes of the type $|00\rangle \longleftrightarrow |1,-1\rangle$ involving two spins (see Appendix A). We thus simulate the dynamics of the spin-1 model via a time-dependent cluster-mean-field (CMF) approach with clusters containing two spins along the y axis [Fig. 1(a)]. The wave function of the μth cluster is written as

$$|\psi\rangle_\mu = \sum_{l,l'} \alpha_{ll'}^{(\mu)} |l\rangle_{1\mu} |l'\rangle_{2\mu}, \tag{10}$$

where $l,l' = -1, 0, 1$, the indices 1 and 2 label the particles in the cluster, and $\alpha_{ll'}^{(\mu)}$ are the variational parameters subject to the normalization constraint $\sum_{l,l'} |\alpha_{ll'}^{(\mu)}|^2 = 1$. The corresponding *Ansatz* for the wave function of the system is a product state

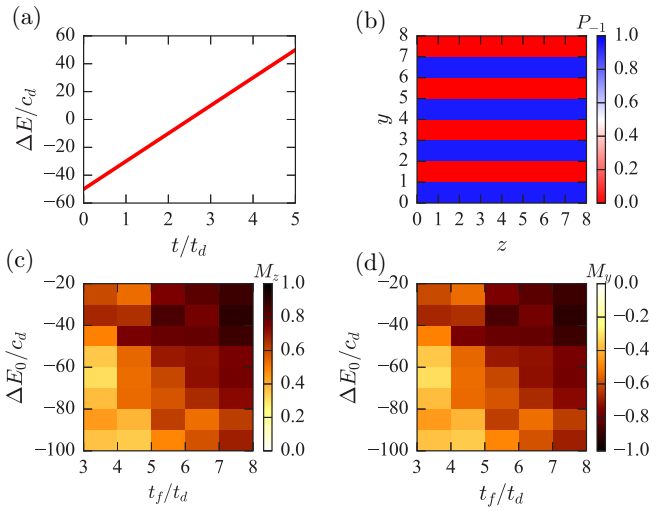

FIG. 5. (a) Time dependence of ΔE used for the preparation of the stripe phase. (b) Occupation of state $|-1\rangle$, P_{-1}, showing the stripe phase formed on an 8×8 lattice at the end of the linear ramp from (a). The final values of the spin-spin correlations (c) M_z and (d) M_y for the 8×8 lattice as a function of ΔE_0 and t_f with a fixed value of $\Delta E_f = 50c_d$.

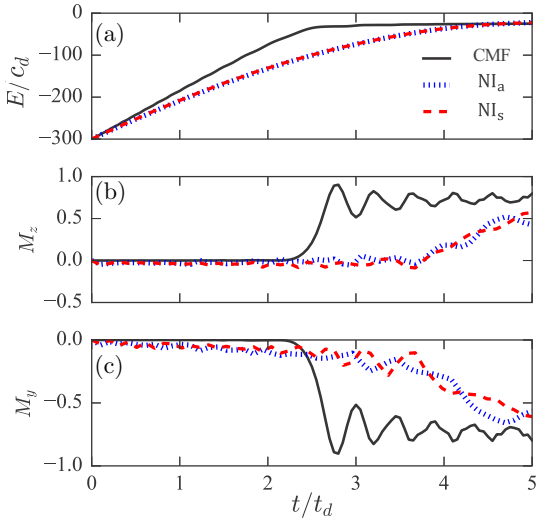

FIG. 6. Time evolution of (a) the energy E, (b) M_z, and (c) M_y on a 3×4 lattice for the spin-1 model. The solid lines shows the results of the CMF, and the red dashed ($\mathrm{NI_s}$) and blue dotted ($\mathrm{NI_a}$) lines are the results of the NI in the presence and absence of the symmetry-breaking term H_{SB}, respectively.

of all clusters,

$$|\Phi\rangle = \prod_{\mu=1}^{N/2} |\psi\rangle_\mu. \tag{11}$$

Based on this *Ansatz* and the Hamiltonian (2), we construct the Lagrangian (7) and the corresponding Euler-Lagrange equations describing the time evolution of the variational parameters $\alpha_{ll'}^{(\mu)}$, which are rather lengthy and presented in Appendix B.

We now apply this scheme to study the dynamical preparation of the stripe phase with the linear ramp of $\Delta E(t)$. We consider in the following the parameters of the Hamiltonian (2) to be $\beta = -2.75$, $\gamma = -1.85$, and $\delta = -1.25$, corresponding to the case of our implementation with erbium atoms. In doing the calculations, we also add the term

$$H_{\mathrm{SB}} = \sum_\mu \epsilon(t)(|1\rangle_{1\mu}\langle 1|_{1\mu} - |1\rangle_{2\mu}\langle 1|_{2\mu}) \tag{12}$$

to the Hamiltonian (2), where $\epsilon(t)$ is the small energy shift [$\epsilon(t_f) = 0$] between the two sites (and therefore between states $|-1,1\rangle$ and $|1,-1\rangle$) in each cluster, to break the up-down symmetry and obtain the stripe phase (Appendix B). Further details and the results of the calculations on an 8×8 lattice are presented in Fig. 5. Figure 5(a) shows an example of the function $\Delta E(t)$ we used for the state preparation. In Fig. 5(b) we present the occupation of state $|-1\rangle$ at the end of evolution starting initially from state $|G'\rangle$, which clearly shows the formation of the stripe phase. For the final value $\Delta E_f = 50c_d$, the spin-spin correlations M_z and M_y in the final state are shown in Figs. 5(c) and 5(d), respectively, as a function of ΔE_0 and final time of evolution t_f. One clearly sees the effect of the speed of the ramp on the fidelity of the state preparation.

Finally, in Fig. 6 we compare the results of the time-dependent CMF (solid lines) with those obtained by direct numerical integration (NI) of the time-dependent Schrödinger equations for the system on a 3×4 lattice. In Fig. 6, the dashed red (dotted blue) line is the result of the NI with (without) the symmetry-breaking term H_{SB} used in the CMF. For all the calculations we used the linear ramp with ΔE changing from $\Delta E_0 = -50c_d$ to $\Delta E_f = 50c_d$ between $t_i = 0$ and $t_f = 5$.

Concerning the final states of the evolution, the results show good agreement between the NI and CMF methods: the energies match within less than 1%, while the spin correlations are overestimated (around 20%) by the CMF method. During the evolution, however, the deviations between the two methods are much more pronounced. This is not a surprise, keeping in mind the simplicity of the wave function in the CMF *Ansatz*, Eqs. (10) and (11), and has the same origin (very limited part of the Hilbert space used in the CMF *Ansatz*) as in the case of the spin-1/2 model discussed above.

IV. MICROSCOPIC REALIZATION OF SPIN MODELS WITH MAGNETIC ATOMS

In this section we present an implementation of the aforementioned spin models on the basis of magnetic atoms, with spin states being encoded in the Zeeman sublevels of the atomic ground state. We note that, being based on generic properties of the DDIs, the models can also be realized in other experimental platforms such as polar molecules [5,34], Rydberg atoms [35,36], and trapped ions [37–39].

The setup we have in mind is represented schematically in Fig. 7 with magnetic atoms placed on a square lattice and prepared in their electronic ground-state manifold. Considering the case of a fine-structure manifold with angular momentum J [40], our two models will involve a restricted number of levels (two and three) compared to the total number of states $2J + 1$ [see Fig. 7(b)].

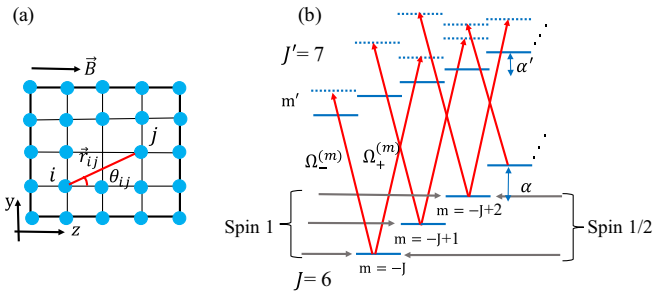

FIG. 7. (a) Magnetic atoms loaded on a square lattice in the presence of an in-plane magnetic field. (b) Level structure of a bosonic erbium atom taken as an example, with the indication of states for realizing spin-1 and spin-1/2 models. Two right- and left-handed circularly polarized laser beams with m-dependent Rabi frequencies $\Omega_\pm^{(m)}$ are used to implement state-dependent energy shifts.

We start by reviewing the basic properties of the DDI between magnetic atoms and then show how to select energetically a particular subset of Zeeman levels to implement our two spin models. Finally, we discuss the resulting relevant time scales for the stripe-phase preparation.

A. Dipole-dipole interactions between magnetic atoms

For two magnetic atoms which are located at sites i and j of a two-dimensional square lattice, the operator of the DDI reads [2]

$$V_{ij} = \frac{c_d}{r_{ij}^3}[\boldsymbol{J}^{(i)} \cdot \boldsymbol{J}^{(j)} - 3(\boldsymbol{J}^{(i)} \cdot \hat{\boldsymbol{r}}_{ij})(\boldsymbol{J}^{(j)} \cdot \hat{\boldsymbol{r}}_{ij})], \tag{13}$$

with $c_d = \mu_0(g_J\mu_B)^2/(4\pi a^3)$, where μ_0 is the magnetic permeability of the vacuum, μ_B is the Bohr magneton, g_J is the Landé factor, $J^{i(j)}$ denotes the operator of the total angular momentum of particle i (j), and $\boldsymbol{r}_{ij} = \boldsymbol{r}_i - \boldsymbol{r}_j$ is the relative position of two particles ($\hat{\boldsymbol{r}}_{ij} = \boldsymbol{r}_{ij}/r_{ij}$) in units of the lattice spacing a. Assuming the presence of a strong external magnetic field $\mathbf{B} = B\hat{\mathbf{z}}$ and choosing its direction as the quantization axis, the DDI Hamiltonian can be written as [41]

$$H_{\rm int} = H_{q=0} + H_{q=1} + H_{q=2}, \tag{14}$$

where the first term,

$$H_{q=0} = \sum_{i<j} J_{ij}\left[J_z^{(i)}J_z^{(j)} - \frac{1}{4}(J_+^{(i)}J_-^{(j)} + \text{H.c.})\right], \tag{15}$$

conserves the total angular momentum of two atoms. Here $J_{ij} = (c_d/r_{ij}^3)(1 - 3\cos^2\theta_{ij})$, with θ_{ij} being the angle between $\boldsymbol{r}_{ij}$ and the z axis. The second and last terms of the Hamiltonian (14) are

$$H_{q=1} = -\frac{3}{2}\sum_{i\neq j}\frac{c_d}{r_{ij}^3}\sin\theta_{ij}\cos\theta_{ij}\left(J_+^{(i)}J_z^{(j)}e^{-i\phi_{ij}} + \text{H.c.}\right), \tag{16}$$

$$H_{q=2} = -\frac{3}{4}\sum_{i<j}\frac{c_d}{r_{ij}^3}\sin^2\theta_{ij}(J_+^{(i)}J_+^{(j)}e^{-2i\phi_{ij}} + \text{H.c.}), \tag{17}$$

where $J_\pm = J_x \pm iJ_y$ and ϕ_{ij} is the azimuthal angle of $\boldsymbol{r}_{ij}$ in the x-y plane. These terms do not conserve energy and transfer one ($H_{q=1}$) or two ($H_{q=2}$) units of the internal angular momentum of the atoms to or from their relative orbital motion. In this work, we consider only the term $H_{q=0}$, assuming the Zeeman splitting induced by the magnetic field to be much larger than the DDI, which makes the contribution of nonangular momentum-conserving terms $H_{q\neq0}$ negligible.

B. State-dependent energy shifts

To exclude energetically all unwanted states from the dynamics, we use ac Stark shifts in combination with the linear Zeeman shifts. To this end we consider two polarized laser beams with polarization $\sigma_\pm$ and the same frequency ω, which couple off resonantly states $|m\rangle \equiv |J,m_J\rangle$ of the ground-state manifold to a manifold of excited states $|m'\rangle \equiv |J',m'_J\rangle$, as shown in Fig. 7. The corresponding Hamiltonian within the rotating-wave approximation and in the frame rotating with the laser frequency ω is given by

$$h_J = \sum_{m'=-J'}^{J'}(\alpha' m' - \Delta)|m'\rangle\langle m'| + \sum_{m=-J}^{J}\alpha m|m\rangle\langle m| + \sum_m \Omega_\pm^{(m)}[|(m\pm1)'\rangle\langle m| + \text{H.c.}], \tag{18}$$

where different Landé factors in the two manifolds give rise to different Zeeman shifts $\alpha^{(\prime)} = \mu_B g_{J^{(\prime)}}B$. We note that the Rabi frequencies $\Omega_\pm^{(m)} = \Omega_\pm C_\pm^{(m)}$ depend on m due to the different Clebsch-Gordan coefficients $C_\pm^{(m)}$ involved in the electric dipole transitions. Finally, $\Delta = \omega - \omega_0$ is the detuning, where ω_0 denotes the resonant frequency between the ground and the first excited states in the absence of the magnetic field. Taking the laser coupling as a perturbation [$|\Delta - \alpha'(m\pm1) + \alpha m| \gg \Omega_\pm^{(m)}$], the effective Hamiltonian for the ground-state manifold in the second-order perturbation theory can be written as

$$h_J = \sum_{m=-J}^{J}(\alpha m + \epsilon_m)|m\rangle\langle m|, \tag{19}$$

where $\epsilon_m = \frac{\Omega_+^{(m)2}}{\Delta-\alpha'(m+1)+\alpha m} + \frac{\Omega_-^{(m)2}}{\Delta-\alpha'(m-1)+\alpha m}$. (Note that we neglected the two-photon Raman transitions $|m\rangle \to |m+2\rangle$ assuming $\alpha,\Delta \gg \Omega_\pm^{(m)}$.) The ac Stark shifts ϵ_m depend nonlinearly on m, which will allow energy-conserving dynamics only on a restricted set of two (three) Zeeman states in the ground-state manifold for the spin-1/2 (spin-1) model. We also note that an alternative way to realize the nonlinear energy shifts is by using the quadratic Zeeman effect.

C. Implementation of the spin-1 model

Following the discussion above, the effective Hamiltonian governing the dynamics on the ground-state manifold has the form $H = H_{q=0} + h_J$. To implement the spin-1 model described in Sec. II B, we consider, for example, the three adjacent magnetic levels $|m = m_0 - 1, m_0, m_0 + 1\rangle$, with $m_0 = -J + 1$ (Fig. 7; another option would be $m_0 = J - 1$). We then impose the condition $|2\epsilon_{m_0+1} - \epsilon_{m_0} - \epsilon_{m_0+2}| \gg c_d$, which suppresses the process $|m_0 + 1, m_0 + 1\rangle \to |m_0, m_0 + 2\rangle$ (due to $H_{q=0}$) energetically, to make only

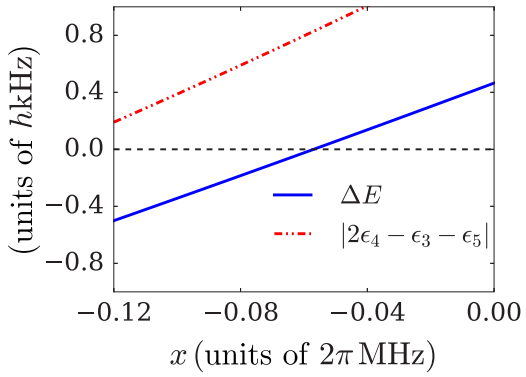

FIG. 8. The control parameter in the spin-1 model ΔE (blue line) for erbium atoms, which changes from a negative value to a positive one to prepare the stripe phase at the end. The energy shift for the transition $|m=-4,m=-4\rangle \longleftrightarrow |m=-5,m=-3\rangle$ (red dash-dotted line), which is forbidden because it is much larger than $c_d = 2\pi \times 0.9\hbar$ Hz. Note that here $\Omega_\pm = 2\pi \times 0.5\,\text{MHz} \pm x$, $\Delta = 0.8\alpha$, and the applied magnetic field is $B = 5$G.

the levels $|m = m_0 - 1, m_0, m_0 + 1\rangle$ accessible. One can now use the projector $P = |m_0 - 1\rangle\langle m_0 - 1| + |m_0\rangle\langle m_0| + |m_0 + 1\rangle\langle m_0 + 1|$ and write the resulting Hamiltonian with the corresponding spin-1 operators, as defined in Sec. II B. This gives the interaction terms of Eq. (2) with the parameters $\beta = -J_1^2/8$, $\gamma = -J_1(J_1 - J_2)/8$, and $\delta = -(J_1 - J_2)^2/8$, with $J_1 = \sqrt{J(J+1) - m_0(m_0+1)}$ and $J_2 = \sqrt{J(J+1) - m_0(m_0-1)}$. The only remaining term is the single particle energy term, h_J, which takes the form of the first term in Eq. (2), provided one changes the frame to $|k\rangle = |m = m_0 + k\rangle e^{-i(\alpha(m_0+k)+\epsilon_{m_0+k} - \Delta E/2\delta_{k,0})t}$, with $k = -1, 0, 1$ and $\Delta E = 2\epsilon_{m_0} - \epsilon_{m_0-1} - \epsilon_{m_0+1}$. Note that the energy shift ΔE can be varied in time by using the time-dependent Rabi frequencies $\Omega_\pm$ and the detuning Δ. As an example, we consider ground-state bosonic erbium atoms with $J = 6$ [42] ($g_J = 1.1638$ [43]), which are trapped in a square lattice with lattice spacing $a = 266$ nm [11]. This results in the dipole-dipole coupling $c_d = 2\pi \times 0.9\hbar$ Hz. In order to satisfy the requirements above for preparing the stripe phase for the case of erbium atoms with $m_0 = -5$, one can apply two laser beams with the Rabi frequencies $\Omega_\pm = 2\pi \times 0.5\,\text{MHz} \pm x$ and the detuning $\Delta = 0.8\alpha$, which couple the ground-state manifold to the manifold with $J' = 7$ ($g_{J'} = 1.070$). In the presence of a magnetic field $B = 5$G ($\alpha = 51.186\hbar$ MHz and $\alpha' = 47.06\hbar$ MHz), we get Fig. 8, which shows all the requirements are fulfilled.

Finally, we emphasize that the spin-1 model involves only magnetization conserving terms and is thus robust (first order in the Zeeman shifts) against time-dependent fluctuations of the magnetic field. This is not the case for the spin-1/2 model discussed below.

D. Implementation of the spin-1/2 model

The spin-1/2 model can be implemented by choosing two states, $|m = -J\rangle$, and $|m = -J + 2\rangle$, in the ground-state manifold as spin states, $|-J\rangle = |\uparrow\rangle$ and $|-J+2\rangle = |\downarrow\rangle$ (see Fig. 7). To exclude the other Zeeman states from the dynamics, we require the conditions $|\epsilon_{-J} + \epsilon_{-J+2} - 2\epsilon_{-J+1}| \gg c_d$ and $|\epsilon_{-J+3} + \epsilon_{-J+1} - 2\epsilon_{-J+2}| \gg c_d$. The resulting projection of the Hamiltonian $H_{q=0}$ onto the submanifold $|-J+2\rangle, |-J\rangle$ leads to the first term in Eq. (1). To obtain the other terms we can use an additional Raman coupling of states $|-J\rangle$ and $|-J+2\rangle$. In the rotating-wave approximation, this coupling takes the form of the two magnetic fields Ω and Δ which appear in (1) [44]. For the purpose of the adiabatic state preparation, these fields can be controlled by changing the Rabi frequency and the detuning of the additional Raman coupling (see, for example, [7]).

E. Time scales

With the above implementation schemes in mind, we can now estimate the time scales required for our state-preparation protocol under realistic experimental conditions. Coming back to the previously discussed example, i.e., erbium atoms, one gets $2\pi \times 3.66\hbar$ Hz for the exchange interaction. This gives $t_f < 1$ s for the time required to adiabatically prepare the stripe phase in the spin-1 case ($t_d \sim 0.177$ s), which is very compatible with experimental time scales. (For the spin-1/2 case, the required time is an order of magnitude larger, which does not look realistic.) We also note that the Raman couplings involved in the implementation of the models give rise to decoherence with the rate $\Gamma \sim (\frac{\Omega}{\Delta})^2 \Gamma_r$, where Γ_r is the linewidth of the excited states involved. This rate should be much smaller than the exchange interaction, which requires $\Delta \gg \Omega, \Gamma_r$ [16,45,46].

V. CONCLUSION

We have shown how systems of magnetic atoms in optical lattices can be used to realize stripe phases in current experiments. On the methodological side, we have employed time-dependent variational *Ansätze* which, as also reported in [29], seem particularly well suited to address adiabatic state preparation for magnetically ordered states. Most importantly, they enable the investigation of systems sizes comparable to current cold-atom experiments, which is well beyond what can be reached with exact methods. We remark that our many-body results can find immediate applications to other physical settings, such as polar molecules and Rydberg atoms in optical lattices [2] and superconducting qubits [24,25], where both Heisenberg-type and Ising Hamiltonians with dipolar interactions can be realized.

Our results show how the combination of long coherence times and flexibility in initializing and manipulating magnetic atoms represents an ideal tool to explore quantum magnetism, despite the interaction strengths being weaker (in absolute value) with respect to polar molecules and Rydberg gases. Moreover, the tunability of the magnetic-field orientation and strength and the properties of the DDIs also allow us, in principle, to realize other interesting quantum phases, such as integer or fractional Chern insulators [47–51], for which it would be intriguing to formulate a proper time-dependent variational principle to correctly reproduce the exact dynamics.

ACKNOWLEDGMENTS

We acknowledge inspiring and fruitful discussions with P. Zoller. We also thank S. Baier, J. H. Becher, L. Chomaz, F. Ferlaino, M. J. Mark, and G. Natale for helpful discussions

on several aspects of the implementation schemes. The exact diagonalization simulations were performed using the QuTiP toolbox [52]. Research in Innsbruck is supported by the European Research Council (ERC) Synergy Grant UQUAM, EU H2020 FET Proactive projects RySQ, and the Austrian Science Fund through SFB FOQUS (FWF Project No. F4016-N23).

APPENDIX A: EQUATIONS OF MOTION OF THE SPIN-1 MODEL WITHIN THE TIME-DEPENDENT MEAN FIELD

Here we demonstrate that the time-dependent MF approach for the spin-1 model cannot describe the dynamics of the system. Having three available states, $|-1\rangle$, $|0\rangle$, and $|1\rangle$, for each atom, one can start from the product state as

$$|\Phi\rangle = \prod_{i=1}^{N} \sum_{l} \alpha_{l,i} |l\rangle_i, \tag{A1}$$

where $l = -1,0,1$ and the coefficients $\alpha_{l,i}$ are the variational parameter of state $|l\rangle$ of spin i. With this *Ansatz*, the Euler-Lagrange equations for the Lagrangian (7) corresponding to the Hamiltonian (2) read

$$\begin{aligned}
-i\dot{\alpha}^i_{-1} &= \alpha^i_{-1} \sum_j C_{ij}\left(|\alpha^j_1|^2 - |\alpha^j_{-1}|^2\right) \\
&\quad + \frac{\alpha^i_0}{4} \sum_j C_{ij}\left(J_2^2 \alpha_0^{j*} \alpha^j_{-1} + J_1 J_2 \alpha_1^{j*} \alpha^j_0\right) \\
-i\dot{\alpha}^i_0 &= -\alpha^i_0 \Delta E + \frac{\alpha^i_1}{4} \sum_j C_{ij}\left(J_1^2 \alpha_1^{j*} \alpha^j_0 + J_1 J_2 \alpha_0^{j*} \alpha^j_{-1}\right) \\
&\quad + \frac{\alpha^i_{-1}}{4} \sum_j C_{ij}\left(J_2^2 \alpha_{-1}^{j*} \alpha^j_0 + J_1 J_2 \alpha_0^{j*} \alpha^j_1\right) \\
-i\dot{\alpha}^i_1 &= \alpha^i_1 \sum_j C_{ij}\left(|\alpha^j_{-1}|^2 - |\alpha^j_1|^2\right) \\
&\quad + \frac{\alpha^i_0}{4} \sum_j C_{ij}\left(J_1^2 \alpha_0^{j*} \alpha^j_1 + J_1 J_2 \alpha_{-1}^{j*} \alpha^j_0\right).
\end{aligned} \tag{A2}$$

Note that in the Hamiltonian (2), we have used $\beta = -J_1^2/8$, $\gamma = -J_1(J_1 - J_2)/8$, and $\delta = -(J_1 - J_2)^2/8$, with $J_1 = \sqrt{22}$ and $J_2 = \sqrt{12}$. It is easy to see that state $|G'\rangle$ (the initial state in our stripe-phase preparation) with $\alpha^i_{\pm 1}(t_i) = 0$ and $\alpha^i_0(t_i) = 1$ is the eigenstate of the above system of equations: $|G'(t)\rangle = \exp[-iN\Delta E(t - t_i)]|G'\rangle$. On the other hand, state $|G'\rangle$ is not the eigenstate of the Hamiltonian (2) because of the flip-flop processes of the type $|00\rangle \leftrightarrow |1,-1\rangle$ resulting from the term $S^{(i)}_+ S^{(j)}_- + S^{(i)}_- S^{(j)}_+$ in Eq. (2). Not being able to incorporate these processes, the MF approach fails in describing the evolution of the system.

APPENDIX B: DYNAMICS OF THE SPIN-1 MODEL WITHIN TIME-DEPENDENT CLUSTER MEAN FIELD

We here present details about the dynamical CMF approach for the spin-1 model within the *Ansatz* (11). The corresponding Euler-Lagrange equations can be written in the following matrix form:

$$\frac{d}{dt}\alpha_\mu = C\alpha_\mu, \tag{B1}$$

with α_μ being the nine-component vector made of the variational parameters for the μth cluster [see Eq. (10)], $\alpha_\mu = (\alpha_{1,1},\alpha_{1,0},\alpha_{1,-1},\alpha_{0,1},\alpha_{0,0},\alpha_{0,-1},\alpha_{-1,1},\alpha_{-1,0},\alpha_{-1,-1})^\dagger_\mu$, and

$$C = \begin{bmatrix}
C_0 & J_1A^* & 0 & J_1B^* & 0 & 0 & 0 & 0 & 0 \\
J_1A & C_1 & J_2A^* & \frac{J_1^2}{4} & J_1B^* & 0 & 0 & 0 & 0 \\
0 & J_2A & C_2 & 0 & \frac{J_1J_2}{4} & J_1B^* & 0 & 0 & 0 \\
J_1B & \frac{J_1^2}{4} & 0 & C_3 & J_1A^* & 0 & J_2B^* & 0 & 0 \\
0 & J_1B & \frac{J_1J_2}{4} & J_1A & C_4 & J_2A^* & \frac{J_1J_2}{4} & J_2B^* & 0 \\
0 & 0 & J_1B & 0 & J_2A & C_5 & 0 & \frac{J_2^2}{4} & J_2B^* \\
0 & 0 & 0 & J_2B & \frac{J_1J_2}{4} & 0 & C_6 & J_1A^* & 0 \\
0 & 0 & 0 & 0 & J_2B & \frac{J_2^2}{4} & J_1A & C_7 & J_2A^* \\
0 & 0 & 0 & 0 & 0 & J_2B & 0 & J_2A & C_8
\end{bmatrix}, \tag{B2}$$

where

$$\begin{aligned}
A &= \sum_\nu \left[\frac{\gamma_{3\nu}}{2}\left(C^{21}_{\mu\nu} + C^{12}_{\mu\nu}\right) + C^{22}_{\mu\nu}\gamma_{4\nu}\right], \\
B &= \sum_\nu \left[\frac{\gamma_{4\nu}}{2}\left(C^{21}_{\mu\nu} + C^{12}_{\mu\nu}\right) + C^{11}_{\mu\nu}\gamma_{3\nu}\right],
\end{aligned}$$

$$\begin{aligned}
C_0 &= \sum_\nu \left[-\frac{\gamma_{1\nu}+\gamma_{2\nu}}{2}\left(C^{21}_{\mu\nu}+C^{12}_{\mu\nu}\right) - C^{11}_{\mu\nu}\gamma_{1\nu} - C^{22}_{\mu\nu}\gamma_{2\nu}\right] - 1, \\
C_1 &= \sum_\nu \left[-C^{11}_{\mu\nu}\gamma_{1\nu} - \frac{\gamma_{2\nu}}{2}\left(C^{21}_{\mu\nu} + C^{12}_{\mu\nu}\right)\right] - \Delta E + \epsilon,
\end{aligned}$$

$$
\begin{aligned}
C_2 &= \sum_\nu \left[-\frac{(\gamma_{2\nu}-\gamma_{1\nu})}{2}\left(C^{21}_{\mu\nu}+C^{12}_{\mu\nu}\right) - C^{11}_{\mu\nu}\gamma_{1\nu} + C^{22}_{\mu\nu}\gamma_{2\nu} \right] + 1 + \epsilon, \\
C_3 &= \sum_\nu \left[-C^{22}_{\mu\nu}\gamma_{2\nu} - \frac{\gamma_{1\nu}}{2}\left(C^{21}_{\mu\nu}+C^{12}_{\mu\nu}\right) \right] - \Delta E - \epsilon, \\
C_4 &= -2\Delta E, \\
C_5 &= \sum_\nu \left[C^{22}_{\mu\nu}\gamma_{2\nu} + \frac{\gamma_{1\nu}}{2}\left(C^{21}_{\mu\nu}+C^{12}_{\mu\nu}\right) \right] - \Delta E, \\
C_6 &= \sum_\nu \left[\frac{(\gamma_{2\nu}-\gamma_{1\nu})}{2}\left(C^{21}_{\mu\nu}+C^{12}_{\mu\nu}\right) + C^{11}_{\mu\nu}\gamma_{1\nu} - C^{22}_{\mu\nu}\gamma_{2\nu} \right] + 1 - \epsilon, \\
C_7 &= \sum_\nu \left[C^{11}_{\mu\nu}\gamma_{1\nu} + \frac{\gamma_{2\nu}}{2}\left(C^{21}_{\mu\nu}+C^{12}_{\mu\nu}\right) \right] - \Delta E, \\
C_8 &= \sum_\nu \left[\frac{(\gamma_{2\nu}+\gamma_{1\nu})}{2}\left(C^{21}_{\mu\nu}+C^{12}_{\mu\nu}\right) + C^{11}_{\mu\nu}\gamma_{1\nu} + C^{22}_{\mu\nu}\gamma_{2\nu} \right] - 1.
\end{aligned}
\tag{B3}
$$

The coefficients $C^{l,l'}_{\mu\nu} = (1 - 3\cos^2\theta^{l,l'}_{\mu,\nu}) r^{-3}_{\mu\nu}$ correspond to the dipole-dipole coupling between the lth particle of the μth cluster and the l'th particle of the νth cluster. We have also defined

$$
\begin{aligned}
\gamma_{1\nu} &= \sum_{l=-1}^{1} \left(\left|\alpha^\nu_{1,l}\right|^2 - \left|\alpha^\nu_{-1,l}\right|^2 \right), \\
\gamma_{2\nu} &= \sum_{l=-1}^{1} \left(\left|\alpha^\nu_{l,1}\right|^2 - \left|\alpha^\nu_{l,-1}\right|^2 \right), \\
\gamma_{3\nu} &= \frac{1}{4}\sum_{l=-1}^{1} \left(J_2 \alpha^\nu_{-1,l}\alpha^{\nu^*}_{0,l} + J_1 \alpha^\nu_{0,l}\alpha^{\nu^*}_{1,l} \right), \\
\gamma_{4\nu} &= \frac{1}{4}\sum_{l=-1}^{1} \left(J_2 \alpha^\nu_{l,-1}\alpha^{\nu^*}_{l,0} + J_1 \alpha^\nu_{l,0}\alpha^{\nu^*}_{l,1} \right).
\end{aligned}
\tag{B4}
$$

Note that in Sec. III B we introduced the (time-dependent) energy difference ϵ between states $|1,-1\rangle$ and $|-1,1\rangle$ in each cluster to break the symmetry between them, which prevents the dynamical formation of the stripe phase. The inclusion of ϵ, for which we assume a decaying time dependence, breaks the translational symmetry and results in the formation of the stripe phase.

[1] M. A. Baranov, M. Dalmonte, G. Pupillo G, and P. Zoller, Chem. Rev. **112**, 5012 (2012).
[2] T. Lahaye, C. Menotti, L. Santos, M. Lewenstein, and T. Pfau, Rep. Prog. Phys. **72**, 126401 (2009).
[3] A. Browaeys, D. Barredo, and T. Lahaye, J. Phys. B **49**, 152001 (2016).
[4] A. de Paz, A. Sharma, A. Chotia, E. Maréchal, J. H. Huckans, P. Pedri, L. Santos, O. Gorceix, L. Vernac, and B. Laburthe-Tolra, Phys. Rev. Lett. **111**, 185305 (2013).
[5] B. Yan, S. A. Moses, B. Gadway, J. P. Covey, K. R. A. Hazzard, A. M. Rey, D. S. Jin, and J. Ye, Nature (London) **501**, 521 (2013).
[6] N. Malossi, M. M. Valado, S. Scotto, P. Huillery, P. Pillet, D. Ciampini, E. Arimondo, and O. Morsch, Phys. Rev. Lett. **113**, 023006 (2014).
[7] P. Schauß, J. Zeiher, T. Fukuhara, S. Hild, M. Cheneau, T. Macrì T, T. Pohl, I. Bloch, and C. Gross, Science **347**, 1455 (2015).
[8] M. F. Parsons, A. Mazurenko, C. S. Chiu, G. Ji, D. Greif, and M. Greiner, Science **353**, 1253 (2016).
[9] M. Boll, T. A. Hilker, G. Salomon, A. Omran, J. Nespolo, L. Pollet, I. Bloch, and C. Gross, Science **353**, 1257 (2016).
[10] L. W. Cheuk, M. A. Nichols, K. R. Lawrence, M. Okan, H. Zhang, E. Khatami, N. Trivedi, T. Paiva, M. Rigol, and M. W. Zwierlein, Science **353**, 1260 (2016).
[11] S. Baier, M. J. Mark, D. Petter, K. Aikawa, L. Chomaz, Z. Cai, M. A. Baranov, P. Zoller, and F. Ferlaino, Science **352**, 201 (2016).
[12] C. Lacroix, P. Mendels, and F. Mila, *Introduction to Frustrated Magnetism* (Springer, Berlin, 2011).
[13] S. Jin, A. Sen, W. Guo, and A. W. Sandvik, Phys. Rev. B **87**, 144406 (2013).
[14] P. A. Lee, N. Nagaosa, and X. G. Wen, Rev. Mod. Phys. **78**, 17 (2006).
[15] B. Pasquiou, E. Maréchal, G. Bismut, P. Pedri, L. Vernac, O. Gorceix, and B. Laburthe-Tolra, Phys. Rev. Lett. **106**, 255303 (2011).
[16] A. Frisch, K. Aikawa, M. Mark, A. Rietzler, J. Schindler, E. Zupanič, R. Grimm, and F. Ferlaino, Phys. Rev. A **85**, 051401(R) (2012).
[17] I. Ferrier-Barbut, H. Kadau, M. Schmitt, M. Wenzel, and T. Pfau, Phys. Rev. Lett. **116**, 215301 (2016).
[18] T. Lahaye, T. Koch, B. Fröhlich, M. Fattori, J. Metz, A. Griesmaier, S. Giovanazzi, and T. Pfau, Nature (London) **448**, 672 (2007).
[19] M. Lu, N. Q. Burdick, and B. L. Lev, Phys. Rev. Lett. **108**, 215301 (2012).
[20] J. Li, J. Lee, W. Huang, S. Burchesky, B. Shteynas, F. Ç. Top, A. O. Jamison, and W. Ketterle, Nature **543**, 91 (2017).
[21] Y. Zhang, L. Mao, and C. Zhang, Phys. Rev. Lett. **108**, 035302 (2012).
[22] Y. Li, L. P. Pitaevskii, and S. Stringari, Phys. Rev. Lett. **108**, 225301 (2012).
[23] C. Gross and I. Bloch, Annu. Rev. Cold At. Mol. **3**, 181 (2015).
[24] M. Dalmonte, S. I. Mirzaei, P. R. Muppalla, D. Marcos, P. Zoller, and G. Kirchmair, Phys. Rev. B **92**, 174507 (2015).
[25] O. Viehmann, J. von Delft, and F. Marquardt, Phys. Rev. Lett. **110**, 030601 (2013).
[26] If the quantization axis is perpendicular to the lattice, the angle θ_{ij} is fixed to $\pi/2$ for all atomic pairs.
[27] H. Weimer and H. P. Büchler, Phys. Rev. Lett. **105**, 230403 (2010).
[28] E. Sela, M. Punk, and M. Garst, Phys. Rev. B **84**, 085434 (2011).
[29] B. Vermersch, M. Punk, A. W. Glaetzle, C. Gross, and P. Zoller, New J. Phys **17**, 013008 (2015).

[30] L. Rademaker, Y. Pramudya, J. Zaanen, and V. Dobrosavljević, Phys. Rev. E **88**, 032121 (2013).
[31] T. Pohl, E. Demler, and M. D. Lukin, Phys. Rev. Lett. **104**, 043002 (2010).
[32] J. Schachenmayer, I. Lesanovsky, A. Micheli, and A. J. Daley, New J. Phys. **12**, 103044 (2010).
[33] P. Kramer, J. Phys. Conf. Ser. **99**, 012009 (2008).
[34] S. R. Manmana, E. M. Stoudenmire, K. R. A. Hazzard, A. M. Rey, and A. V. Gorshkov, Phys. Rev. B **87**, 081106(R) (2013).
[35] M. Saffman, T. G. Walker, and K. Mølmer, Rev. Mod. Phys. **82**, 2313 (2010).
[36] H. Weimer, M. Müller, I. Lesanovsky, P. Zoller, and H. P. Büchler, Nat. Phys. **6**, 382 (2010).
[37] K. Kim, M. S. Chang, S. Korenblit, R. Islam, E. E. Edwards, J. K. Freericks, G. D. Lin, L. M. Duan, and C. Monroe, Nature (London) **465**, 590 (2010).
[38] P. Richerme, Z.-X. Gong, A. Lee, C. Senko, J. Smith, M. Foss-Feig, S. Michalakis, A. V. Gorshkov, and C. Monroe, Nature (London) **511**, 198 (2014).
[39] P. Jurcevic, B. P. Lanyon, P. Hauke, C. Hempel, P. Zoller, R. Blatt, and C. F. Roos, Nature (London) **511**, 202 (2014).
[40] We consider, for simplicity, the absence of hyperfine interactions.
[41] L. Santos and T. Pfau, Phys. Rev. Lett. **96**, 190404 (2006).
[42] The hyperfine structure is absent in this case.
[43] J. G. Conway and B. G. Wybourne, Phys. Rev. **130**, 2325 (1963).
[44] Note that we can neglect the transition between other ground-state levels $|m\rangle$ assuming that the Landé factors between ground (J) and excited manifolds allow us to make a state-selective Raman transition between $|-J+2\rangle$ and $|-J\rangle$.
[45] J. Marek and H. Stahnke, Z. Phys. A **298**, 81 (1980).
[46] A. Frisch, K. Aikawa, M. Mark, F. Ferlaino, E. Berseneva, and S. Kotochigova, Phys. Rev. A **88**, 032508 (2013).
[47] N. Y. Yao, C. R. Laumann, A. V. Gorshkov, S. D. Bennett, E. Demler, P. Zoller, and M. D. Lukin, Phys. Rev. Lett. **109**, 266804 (2012).
[48] N. Y. Yao, A. V. Gorshkov, C. R. Laumann, A. M. Läuchli, J. Ye, and M. D. Lukin, Phys. Rev. Lett. **110**, 185302 (2013).
[49] S. V. Syzranov, M. L. Wall, V. Gurarie, and A. M. Rey, Nat. Commun. **5**, 5391 (2014).
[50] D. Peter, N. Y. Yao, N. Lang, S. D. Huber, M. D. Lukin, and H. P. Büchler, Phys. Rev. A **91**, 053617 (2015).
[51] S. V. Syzranov, M. L. Wall, B. Zhu, V. Gurarie, and A. M. Rey, Nat. Commun. **7**, 13543 (2016).
[52] J. R. Johansson, P. D. Nation, and F. Nori, Comput. Phys. Commun. **184**, 1234 (2013).